Two-dimensional powder diffraction

B. Hinrichsen, R.E. Dinnebier and M. Jansen

The growing attractiveness of two-dimensional detectors in powder diffraction has one severe drawback – the 2D to 1D data reduction. This can be a most time consuming and error prone operation, especially when the artifacts of the sample environment affect the intensities. Some developments in the field of calibrating, filtering and evaluation are presented.

Introduction: The combination of two-dimensional detectors, powder diffraction and synchrotron light sources has been staggeringly successful, opening doors to many new experiments [1–5]. The great advantages of such data collection lie in the short exposure times as well as in the huge redundancy. A large angular region of the Bragg cone is recorded in a single exposure; indeed most detectors are set up perpendicular to the primary beam and centered by it, intercepting the Bragg cone over the entire azimuthal range. The standard practice is to integrate the image along the ellipses described by the intersection of the cone with the planar detector to a conventional powder pattern [6]. This commonly reduces the amount of information by the square root of the number of pixels. Does this represent the gamut of information contained in a powder diffraction image? A glance at an image from a calibration standard might lend itself to such a conclusion. Less perfect samples, as well as sample environments leave distinctive artifacts on images. How can they be extracted, filtered or interpreted? Methods offering answers to some of these questions are introduced.

Experimental geometry: The experimental geometry of a plane detector used for powder diffraction has been explained in detail by others [6]. We will therefore merely give a short outline of the most important points. Each diffraction (Bragg) cone intersecting a plane detector results in an elliptical projection (see Fig. 80). This projection is described most palpably using the experimental parameters of the beam centre, the sample to detector distance, the tilt of the detector out of the normal of the primary beam and finally the azimuthal rotation of the tilt with respect to an arbitrarily selected position.

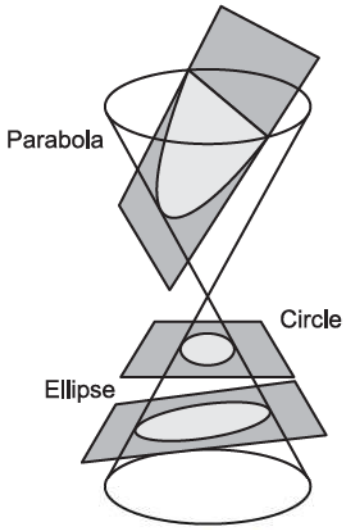

Figure 80: Conic sections. The planes represent the detector plane at various angles to the primary beam. The projections of the Bragg cone trace a circle, an ellipse or a parabola on the detector. In the course of the calibration of the experimental geometry a high-quality image of a standard sample is used to determine and refine the required five parameters.

The standard method for refining the calibration parameters can be separated into two parts. Initially a number of radial lines are drawn from the common focus of the ellipses to the edge of the image. The profile along these lines is plotted, and the peak positions refined using a Gaussian profile. To ensure that an acceptable number of pixels are selected to contribute to the individual histograms the radial lines need to be of an acceptable width, in our case a width of five pixels for these lines returned good results. The peak positions, or rather the positions of the intersection of the radial lines with the ellipses, are now known. Each point can be uniquely associated to a given lattice spacing.

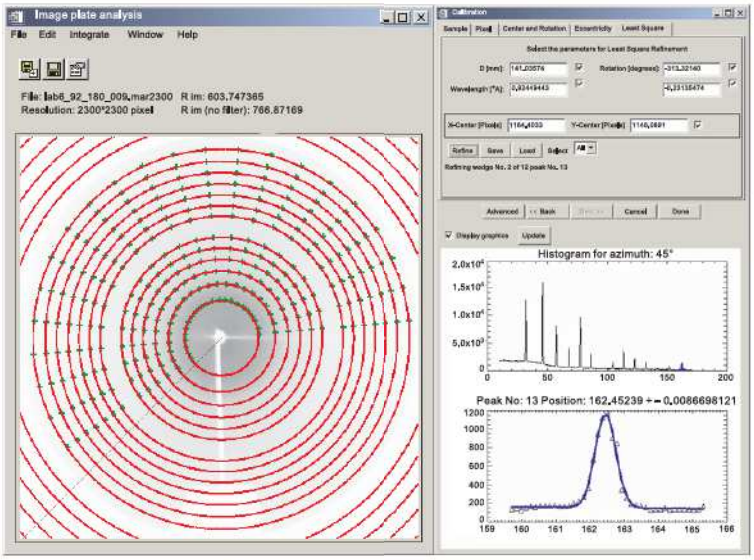

Figure 81: Conventional calibration refinement method. On the left the radial lines are traced from the centre to the edge. The intensity profile is traced and the various peaks are fitted using a Gaussian profile function. The successfully refined peak positions are utilized to refine the five calibration parameters.

The requirement that points belonging to the same lattice spacing should have an identical diffraction angle is sufficient for the refinement of the calibration parameters. A Levenberg-Marquard least squares minimization using the positions weighted by the statistical uncertainty of the initial peak refinement procedure leads to the final calibration values. This method leads to good results if enough radial lines are chosen and the initial six starting values, the five calibration parameters and the wavelength, are sufficiently close to the true values. To ensure this we have developed pattern recognition techniques which very successfully estimate these parameters [7,8]. These have been described elsewhere. Recently an alternative calibration method has been proposed [9] which appears to have a high degree of automation.

Whole image refinement: The question poses itself, especially in view of the great computing power available to us currently, why image analysis is always synonymous with data reduction? Could not far more information be gleaned from diffraction images than a distilled $I(2\theta)$ plot? As a first step along the path of full pattern appreciation this holistic approach was applied to the calibration refinement with surprising results. Calibration, as described earlier, is commonly a two step process. The initial step is the determination of the intersections of any number of radial lines with the Bragg ellipses. The second is the refinement of the ellipse (calibration) parameters along those points (see Fig. 81).

The approach chosen here was to refine the sought after parameters against the difference of the observed and computed *images* (Fig. 82). The number of data points in such a refinement is of course rather large, a couple of million against what would normally be a couple of hundred. As ellipses furthest from the centre are most susceptible to the calibration quality, the FWHM of the highest angle peak of a from the integrated pattern was chosen to give an idea of the calibration results. The material used was the common calibration standard finely ground LaB_6. Whole image refinement showed an improvement over the conventional method of 15%, reducing the FWHM from 0.122° to 0.106°.

Figure 82: Whole image refinement. The observed intensities (I_{obs}) are shown in the left image. In the central image the simulated intensities (I_{calc}) are shown. The difference is shown on the right. The calibration parameters are refined to minimize the difference between I_{obs} and I_{calc}.

Filtering techniques: Experimental artifacts are a continual nuisance in the analysis of *in situ* experiments. These generally result from the experimental environment, can however stem directly from the sample. Data becoming to powder diffraction analysis originates from an ideal sample, having all the positive attributes: random orientation, narrow size dispersion and an improved statistical distribution by sample rotation. In some cases this ideal cannot be achieved, this is especially valid for high-pressure powder diffraction experiments. Sample rotation, if any, is limited to a small angular range because of the diamond diffraction peaks and the deleterious effects of gasket shadowing. An X-ray beam that has a diameter in the order of a few micrometers further worsens the already poor statistics of such an experiment. The general image obtained is filled with single grain spikes looming over the intensity of the Debye-Scherrer ring by at least an order of magnitude. A few peaks on a ring can cause the normal averaging process used during integration to produce data misrepresents the true powder intensities.

When estimating the most representative value for the intensity of a single bin generally only the mean of the intensities within the bin was calculated. This of course leads to great aberrations when outlier intensities are within the bin. One way of dealing with such data would be to select the median value as a more robust estimator of the true intensity. This however still leads to variances which do not portray the true data quality. The sigmas of the intensities, which are generally used to weight the least squares refinements are completely meaningless and of no use in the refinement process.

An alternative method is to filter out the aberrant values. As a rule only very few highly deviant values cause the averaging problems. A method which can be looked upon as the inverse of the aforementioned median intensity estimation is that of fractile filtering. Here a highest or lowest intensity fraction of the data is removed. As this method has no real intensity based cut-off criteria it is very robust. An additional advantage is that it does not skew normally distributed data. The effects of this computationally cheap filter can be seen in Fig. 83, an example of a high-temperature image.

Reliability values: The visual appreciation of a two-dimensional diffraction image can sometimes give an idea of the quality of the data gathered. No quantitative measure of the quality of such a data collection has yet been proposed. In lieu of appraising the effectiveness of the presented filtering algorithms an unbiased estimation of the data quality seemed opportune. A measure that has shown itself to be of good use is shown in Eq.(5).

$$R_{im} = \frac{\frac{1}{n}\sum_{i=1}^{n}\left(\frac{1}{m-1}\sum_{j=1}^{m}(I_j - \bar{I})^2\right)}{\frac{1}{l}\sum_{k=1}^{l}(I_k - I_b)}, \qquad (5)$$

where l is the total number of pixels in the image, n is the number of bins used to integrate the image and m is the number of pixels within each bin.

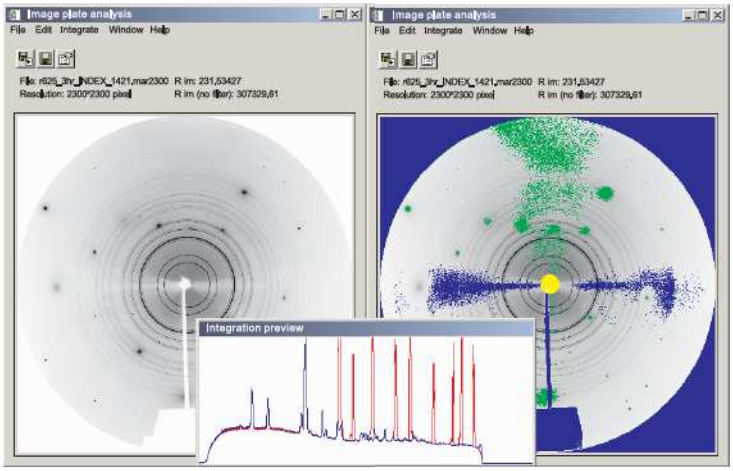

Figure 83: Results of fractile filtering on an image from a high-temperature experiment. Top left: before filtering, top right: after filtering. The spots of high intensity result from the sapphire capillary. The lower image is a preview of the finally integrated diffractogram, red is the unfiltered, blue the filtered pattern.

I_k is the intensity of the k^{th} pixel and I_b the background intensity of that pixel. This is a very simple measure of the average bin variance, normalized to the background corrected total intensity.

Table 2: Image reliability values for some typical examples.

LaB_6	$R_{im} \times 100$ (filter applied)	$R_{im} \times 100$ (no filter)
good calibration	0.414	25.9
bad calibration	10.1	45.9
experimental data		
sapphire tube	1.12	4512
DAC	15.3	7532

The value is intensity and consequently detector independent. It is intentionally very sensitive to azimuthal variations in intensity. This leads to an extremely good indicator of not only the uniformity of the Bragg peaks but also of a successful calibration, as can be seen in Tab. 2.

Concluding remarks: Some aspects in the analysis of two-dimensional powder diffraction patterns have been presented. The effectiveness of filtering methods dealing with outlier intensities has been shown, as has been a holistic approach to the calibration question. Finally an image reliability factor has been proposed to quantify the quality of a diffraction image. All the functionality has been implemented in a freely available software package, Powder3D [10].

[1] *Hanfland, M., U. Schwarz, K. Syassen and K. Takemura.* Physical Review Letters **82**, 1197–1200 (1999).

[2] *Knapp, M., C. Baehtz, H. Ehrenberg and H. Fuess.* Journal of Synchrotron Radiation **11**, 328–334 (2004).

[3] *Norby, P.* Journal of Applied Crystallography **30**, 21–30 (1997).

[4] *Meneghini, C., G. Artioli, A. Balerna, A.F. Gualtieri, P. Norby and S. Mobiliob.* Journal of Synchrotron Radiation **8**, 1162–1166 (2001).

[5] *Wenk, H.R. and S. Grigull.* Journal of Applied Crystallography **36**, 1040–1049 (2003).

[6] *Hammersley, A.P., S.O. Svensson, M. Hanfland, A.N. Fitch and D. Häusermann.* High Pressure Research **14**, 235-248 (1996).

[7] *Hinrichsen, B., R.E. Dinnebier, P. Rajiv, M. Hanfland, A. Grzechnik and M. Jansen.* Journal of Physics: Condensed Matter **18**, 1021–1037 (2006).

[8] *Rajiv, P., B. Hinrichsen, R.E. Dinnebier, M. Joswig and M. Jansen.* Powder Diffraction, in press (2007).

[9] *Cervellino, A., C. Giannini, A. Guagliardi and M. Ladisab.* Journal of Applied Crystallography **39**, 745–748 (2006).

[10] *Hinrichsen, B., R.E. Dinnebier and M. Jansen.* Zeitschrift für Kristallographie **23**, 231–236 (2006).